

---

This is an electronic reprint of the original article.  
This reprint may differ from the original in pagination and typographic detail.

Leppäniemi, Jarmo; Sippola, Perttu; Broas, Mikael; Aromaa, Jari; Lipsanen, Harri; Koskinen, Jari

**Corrosion protection of steel with multilayer coatings: Improving the sealing properties of physical vapor deposition CrN coatings with Al<sub>2</sub>O<sub>3</sub>/ TiO<sub>2</sub> atomic layer deposition nanolaminates**

*Published in:*  
Thin Solid Films

*DOI:*  
[10.1016/j.tsf.2017.02.050](https://doi.org/10.1016/j.tsf.2017.02.050)

Published: 01/04/2017

*Document Version*

Peer-reviewed accepted author manuscript, also known as Final accepted manuscript or Post-print

*Published under the following license:*  
CC BY-NC-ND

*Please cite the original version:*

Leppäniemi, J., Sippola, P., Broas, M., Aromaa, J., Lipsanen, H., & Koskinen, J. (2017). Corrosion protection of steel with multilayer coatings: Improving the sealing properties of physical vapor deposition CrN coatings with Al<sub>2</sub>O<sub>3</sub>/ TiO<sub>2</sub> atomic layer deposition nanolaminates. *Thin Solid Films*, 627, 59-68.  
<https://doi.org/10.1016/j.tsf.2017.02.050>

---

This material is protected by copyright and other intellectual property rights, and duplication or sale of all or part of any of the repository collections is not permitted, except that material may be duplicated by you for your research use or educational purposes in electronic or print form. You must obtain permission for any other use. Electronic or print copies may not be offered, whether for sale or otherwise to anyone who is not an authorised user.

**Corrosion protection of steel with multilayer coatings:  
improving the sealing properties of Physical Vapor Deposition  
CrN coatings with Al<sub>2</sub>O<sub>3</sub>/TiO<sub>2</sub> Atomic Layer Deposition  
nanolaminates**

Jarmo Leppäniemi<sup>a\*</sup>, Perttu Sippola<sup>b\*</sup>, Mikael Broas<sup>c</sup>, Jari

Aromaa<sup>a</sup>, Harri Lipsanen<sup>b</sup> and Jari Koskinen<sup>a</sup>

<sup>a</sup> Department of Material Science, Aalto University School of Chemical Technology,  
P.O. Box 16100, FI-00076 AALTO, Espoo, Finland

<sup>b</sup> Department of Micro- and Nanosciences, Aalto University School of Electrical  
Engineering, P.O. Box 13500, FI-00076 AALTO, Espoo, Finland

<sup>c</sup> Department of Electrical Engineering and Automation, Aalto University School of  
Electrical Engineering, P.O. Box 13500, FI-00076 AALTO, Espoo, Finland

\* The authors contributed equally to this work:

Jarmo Leppäniemi: Tel.: +358 504640143 ; Fax: +358 9 47022659.

E-mail address: jarmo.leppaniemi@aalto.fi

Perttu Sippola: Tel.: +358 408413575 ; Fax:+358 9 4123014.

E-mail address: perttu.sippola@aalto.fi

**Keywords:** corrosion; defects; electrochemical properties; multilayer; PVD ; ALD ;  
thin films ; steel

**Abstract**

Atomic Layer Deposition (ALD) of Al<sub>2</sub>O<sub>3</sub>/TiO<sub>2</sub> nanolaminate was applied to improve the sealing properties of CrN coating deposited with Physical Vapor Deposition (PVD) on high speed steel (HSS). The corrosion protection properties were explored with Linear Sweep Voltammetry and visual estimation. Nearly two orders of magnitude decrease in corrosion current density was obtained by applying plasma pre-

treatment prior to ALD coating. Sealing of CrN pinholes was shown with Focused Ion Beam/Scanning Electron Microscope technique. The effect of the ALD deposition parameters to adhesion of the ALD coatings was investigated with Rockwell indentation and microscope analysis. Thickness and refractive index of the ALD coatings were measured with ellipsometry, and density and roughness of the ALD coatings were investigated with X-Ray Reflectivity measurements. Neutral Salt Spray testing was used to investigate the corrosion resistance of PVD/ALD nanolaminates on HSS dental curettes.

## **1. Introduction**

Steel components and tools face high requirements for both wear and corrosion resistance in many applications. Choosing a harder base steel material can increase the lifetime under heavy load [1-3], but these steel materials are often prone to corrosion or other environmental effects. Physical Vapor Deposition (PVD) coatings are one of the most widely established methods to improve the corrosion protection of steels. For example, CrN-based coatings are used in various applications requiring both corrosion protection and good mechanical properties [4-6]. In aggressive environments, the corrosion protection of CrN coating is generally insufficient as these coatings typically incorporate a large amount of pinholes and defects through which steel material is attacked by corrosion [7-9]. At these defect sites, the smaller area of the less noble steel substrate can lead to extremely high current densities, causing heavy localized corrosion [10].

Recent investigations have focused on applying Atomic Layer Deposition (ALD) to form a protective multilayer complex on steel [11-21]. ALD enables unique thickness control down to molecular level by self-saturating surface reactions of separated,

gaseous source material pulses [22]. This allows conformal and uniform large-area deposition even on 3D morphologies with high aspect ratio structures [23]. Perhaps most promising results with ALD in corrosion protection have been obtained by using them to fill pinholes in PVD coatings [11,12].

While  $\text{Al}_2\text{O}_3$  is most well-known ALD coating that has been shown possess superior sealing properties [18,20], high dissolution rates ( $7 \text{ nm h}^{-1}$  in 0.2 M NaCl) on steel substrate have been reported to limit its use in corrosion protection [24]. ALD nanolaminate films consisting of consecutive thin film layers of two or more binary compounds have been reported to allow combination of the enhanced performance of barrier properties of  $\text{Al}_2\text{O}_3$  with chemical stability from  $\text{TiO}_2$  or  $\text{Ta}_2\text{O}_5$  layers [14,15].

For improved corrosion protection, good adhesion and reduced porosity of the coating, the use of plasma treatments prior to ALD has been reported effective [16]. The benefit of cleaning steel surfaces of contamination with plasma prior to thin film coating was established decades ago [25,26]. In addition, the use of plasma pre-treatment prior ALD deposition has been reported to allow formation of uniform oxide layer, improving growth behavior of  $\text{Al}_2\text{O}_3$  ALD [16,27].

From application point of view, using two different deposition processes with separate equipment imposes a need for very high added value in order to be commercially viable. Considering the economic factors and the major advantage of conformal deposition on 3D morphologies, perhaps most promising future application are medical and dental instruments. In this study we investigate high speed steel (HSS) that has been previously shown superior in orthogonal cutting by dental currettes, when compared to the traditional material choice of martensitic stainless steel [1]. This superior performance allows for increased lifetime and reduced need for re-sharpening. However, as dental currettes are sterilized by autoclaving daily after use, they also

require excellent corrosion resistance. Multilayer CrN/ALD nanolaminate coatings offer potential for corrosion protection of these high-value instruments.

This study focused on investigating the effect of different ALD deposition parameters to improving the corrosion protection of CrN coatings on steel, using Linear Sweep Voltammetry (LSV) measurements and visual estimation. Optical microscope imaging was used to estimate the amount of pinholes on CrN coating before and after the PVD deposition. Energy Dispersive Spectroscopy (EDS), ellipsometry and X-Ray Reflectivity (XRR) measurements were used to investigate the properties of the ALD nanolaminate. In addition, Rockwell indentation was adapted to investigate the adhesion of the ALD coatings on the CrN coating. Focused Ion Beam/Scanning Electron Microscope (FIB/SEM) technique was used to visually investigate the CrN pinholes. Neutral Salt Spray (NSS) testing was employed to investigate the corrosion resistance of multilayer CrN/ALD nanolaminates on steel currettes.

## **2. Experimental details**

The main substrates used in this study were steel disks with a radius and thickness of 1.0 cm. The chemical composition of the HSS is shown in Table 1. The steel disks were hardened and tempered at 1150 °C, resulting in hardness 65 HRC. The surface of the steel disks was turned and polished by an industrial process. This polishing process left a small, 0.25 mm radius pit at the middle of the disk. The surface roughness of the disks was measured by DekTak profilometer. In addition, (100) silicon dies were employed as thickness and density reference samples. Furthermore, dental curette instrument blades were used to visually estimate the conformal deposition of ALD-films to complex 3D-shapes and estimate the corrosion performance of 3D samples in NSS tests.

**Table 1:** Chemical composition (weight percentages) of high speed steel used.

Fe	C	Cr	Mo	V	W	Co
68.10	1.60	4.80	2.00	5.00	10.50	8.00

The CrN coatings used were commercially available BALINIT CNI coatings deposited by sputtering, purchased from Oerlikon Balzers. Prior to the coating, the steel disks were cleaned by an industrial cleaning procedure. The thickness of the coating was approximately 3  $\mu\text{m}$ . After the PVD coating, the steel disks were protected with oil for shipment and storage. The oil was removed prior to taking the samples to cleanroom for ALD by a five minute ultrasonication first in acetone and then in ethanol, followed by wipe-cleaning with 50% solution of isopropanol and DI-water, and finally dried with pressurized nitrogen gas. Just prior to the ALD, the steel samples were cleaned first by 10 minutes in acetone and then in isopropanol solutions in an ultrasonic cleaner. Immediately after cleaning, the samples were transferred into the ALD load lock. The load lock was turbo pumped for 10 minutes to reduce the amount of gaseous impurities.

ALD nanolaminates were deposited with a Picosun R-200 operated on remote inductively coupled plasma (ICP) configuration with a base pressure of 2 mbar. All the depositions were done at 150  $^{\circ}\text{C}$ . Table 2 presents the different ALD runs with varied parameters under study. The default pre-treatment for the sample sets was 10 minutes of continuous  $\text{O}_2$  plasma, with 2500 W RF-power, and 100 sccm carrier  $\text{N}_2$  flow. For  $\text{NH}_3$  plasma sample set,  $\text{N}_2/\text{H}_2$  plasma with 50/50 sccm source gas flows was used instead. During the ALD operation the carrier nitrogen flows into the reactor was 40 sccm from the passive precursor lines (6) and 100 sccm from the plasma line. The ALD nanolaminate master cycle included first, 45 deposition cycles ( $\sim 5$  nm) of trimethylaluminum (TMA,  $\geq 98\%$  purity) and  $\text{H}_2\text{O}$ ; and second, 90 cycles ( $\sim 5$  nm) of

TiCl<sub>4</sub> ( $\geq 98\%$  purity) and H<sub>2</sub>O. The Al<sub>2</sub>O<sub>3</sub> was done by TMA/N<sub>2</sub>/H<sub>2</sub>O/N<sub>2</sub> sequence of 0.2s/5s/0.2s/10s and the TiO<sub>2</sub> by TiCl<sub>4</sub>/N<sub>2</sub>/H<sub>2</sub>O/N<sub>2</sub> sequence of 0.2s/5s/0.2s/10s. The flows for both metal precursor lines were set to 150 sccm and the H<sub>2</sub>O flows were 200 sccm during their pulses. The TMA and TiCl<sub>4</sub> source bottles were kept at a constant temperature of 23 °C.

**Table 2:** ALD nanolaminate coatings deposited on CrN coated high speed steel on different deposition runs. Individual laminate thickness was kept constant at 5 nm.

Code	Plasma pre-treatment	Thickness (nm)
<i>Default</i>	O <sub>2</sub>	50
Noplasma	None	50
NHplasma	N <sub>2</sub> /H <sub>2</sub>	50
t20nm	O <sub>2</sub>	20
t100nm	O <sub>2</sub>	100

The thickness and refractive indices of the ALD thin films were measured with Plasmos SD 2300 ellipsometer from silicon wafer dies. The ellipsometer applied 632.8 nm He-Ne laser as a light source and with 70° angle of incidence. The desired parameters were automatically calculated using single layer mode with effective refractive index value of 2 as an initial value for the iterative data fitting. X-ray reflectivity (XRR) measurements with Phillips X'Pert Pro (Cu-K $\alpha$  wavelength) were performed to analyze the thickness, density and roughness of the deposited thin films (*default*) from silicon die. The XRR measured data was fitted with in-house developed fitting software based on Parrat's formalism. [28] Raman spectroscopy was used to evaluate the crystallinity of the nanolaminates, using a Labram HR (Horiba Jobin-Yvon) system. Argon laser (wavelength = 514nm, power = 10mW) with a BX41 (Olympus)

microscope and 50X objective with spot size less than 1  $\mu\text{m}$  were used. Surface morphologies of the steel disks and CrN coatings were evaluated with scanning electron microscopy (FEGSEM, Tescan Mira3), and energy dispersive spectrometry (EDS) was applied to investigate the CrN and ALD coatings.

Electrochemical properties of coated steel disks were evaluated with polarization measurements using LSV. The measurements were conducted using ACM-Instruments Autotafel potentiostat. A traditional three-electrode setup was utilized with a martensitic stainless steel sheet as the counter electrode (CE), a standard calomel electrode (SCE) as the reference electrode, and the investigated sample as a work electrode (WE). The corrosion potentials were reported with respect to reference electrode. The electrolyte solution was 0.2 M NaCl (Emsure analytical reagent) with pH of 5.2 at room temperature. The measurement range was -1.5 to 0.0 V with a scan rate of 50 mV/min. Exposure area of steel disks was limited to 1.0  $\text{cm}^2$  with Viton O-rings. The steel disks were in contact with salt solution for a total time of 48 hours. During this time, potential sweeps were conducted on three different times, after 1, 24 and 48 hours in the electrolyte. After the 48 h time in salt solution and three potential sweeps, all the samples were visually evaluated for corrosion effects. The corrosion potentials and corrosion current densities were determined by Tafel analysis from polarization curves as described in [29].

In addition to the multilayer-coated steel disks, the corrosion measurements were conducted on steel disks without any coating, steel disks with only CrN coating, and glass rod coated with CrN only. The CrN coated glass rod was used to measure the corrosion current density of the CrN coating itself. To evaluate the performance of the coated HSS and compare it to corrosion resistant high-chromium martensitic stainless steel used in dental currettes [1], a reference set of this martensitic stainless steel was

also investigated. The area of the stainless steel disks and glass rod coated with CrN differed from that of other samples, which was taken into account at the calculation of the corrosion current densities. All tests were repeated three times, except those for glass rod.

The effect of surface irregularities – in the form of the pit at the middle of the disk – to corrosion protection was also evaluated. This was conducted by covering middle pit by lacquer (Duran Schott, Germany). Two sample types were selected for this test: one with CrN coating only and one with multilayer CrN/ALD nanolaminate (*default*). The results of these measurements were compared to non-lacquered ones.

The porosity of the CrN coating was estimated by two methods: optical microscopy area analysis done similarly as presented by Cunha et al. [30], and calculation by corrosion current densities as originally presented by Tato et al. [31] and adapted by Härkönen et al. [21]. In optical microscopy analysis, 50x magnification was used to image the sample surface. The analysis was done for samples with only CrN coating and samples with CrN/ALD nanolaminate (t100nm). Dark spots were observed on the surface of the coating – the area fraction of these dark areas was calculated from the optical microscope images using ImageJ image processing software from a total of 15 images, and standard deviation from different images was used as an error value. These values were then compared to those obtained by calculation by corrosion current densities [31], as given by:

$$P = \left( \frac{i_{coated} - i_{coating}}{i_{substrate}} \right) \times 100\% \quad (1),$$

where  $i_{coated}$  is the corrosion current density of coated steel substrate,  $i_{substrate}$  is the corrosion current density of non-coated steel substrate, and  $i_{coating}$  is the corrosion

current density of the coating itself. For a passive coating,  $i_{coating} \ll i_{substrate}$ , and  $i_{coating}$  can be omitted from the equation [31].

The progression of corrosion and the ALD coating performance to seal pinholes was further evaluated by preparing cross-sectional samples with a dual beam system (FEI Helios NanoLab 600 FIB). One sample with the *default* ALD deposition parameters was chosen for confirmation of pinhole coverage. Two additional samples were chosen for evaluation of corrosion progression: one with a 100 nm ALD nanolaminate and one without. Ion-induced secondary electron channeling contrast was exploited when distinguishing between the steel substrate, CrN coating, possible corrosion products, and the ALD thin film [32].

In addition to the tests with steel disks, corrosion resistance was evaluated with Neutral Salt Spray (NSS) testing for dental cures. This testing was conducted according to EN ISO 9227 procedure, except NaCl concentration was reduced to one fifth ( $10 \text{ g/l} \pm 1 \text{ g/l}$ ) and samples were removed from the chamber, rinsed with deionized water and photographed at regular intervals. Three dental cures were used in this test: one uncoated, one coated with CrN and one coated with CrN/ALD nanolaminate (*default*).

Rockwell indentation was used to measure hardness of uncoated steel discs. Rockwell indentation was also utilized to evaluate CrN coating adhesion of coated steel discs according to VDI 3198 [33] and to visually evaluate the adhesion of ALD coatings by optical microscopy. For the steel disks with the ALD nanolaminates, the indentation was done to disk area at the edge, not exposed to the electrolyte solution. In cases where the inspection indicated that the ALD thin film was completely removed from the vicinity of indentation, EDS analysis was also employed to confirm whether the ALD nanolaminate was completely removed.

### 3. Results and discussion

#### 3.1. Morphology and composition

The CrN coated steel disks had a root-mean-square roughness of 85 nm, averaged from three line scans of two samples. The ALD runs provided good overall uniformity and conformality. The thickness non-uniformity of the ALD nanolaminates were less than 5 % on the six inch wafer area. On the steel disks and instrument blades, the ALD coatings appeared uniform and of similar thickness to that of silicon wafers. Uniformity estimation visually is reasonably accurate to known color changes of TiO<sub>2</sub> by changes in thickness.

The ALD produced repeatable thin film quality with an average effective growth-per-cycle of 0.072 nm/cycle from 8 performed ALD deposition runs, having a standard deviation of 0.003 nm/cycle. The effective refractive indices of the nanolaminates were measured and averaged to be  $2.07 \pm 0.04$ , which coincides with the average of TiO<sub>2</sub> and Al<sub>2</sub>O<sub>3</sub> refractive indices as expected [34]. The ellipsometer measured thickness values were also confirmed reliable by comparing those to XRR analyzed thickness values from the same *default* ALD parameter sample. The XRR analysis yielded total thickness of 44.8 nm, while the ellipsometer produced 46.6 nm. XRR analysis also revealed the average thickness of a single layer of Al<sub>2</sub>O<sub>3</sub> and TiO<sub>2</sub> to be 4 nm and 4.9 nm, respectively. The minor offset between the nominal 50 nm and real thickness can be credited to too low cycle number of the TMA/H<sub>2</sub>O processes.

The densities for the *default* samples were analyzed to be 3.79 g/cm<sup>3</sup> and 2.90 g/cm<sup>3</sup> from averaged TiO<sub>2</sub> and Al<sub>2</sub>O<sub>3</sub> layers, respectively. Both material layers were consistently dense along the whole structure within the typical XRR experimental accuracy of  $\pm 0.05 - 0.1$  g/cm<sup>3</sup> [35]. The XRR extracted nanoscale RMS roughness values were on average 0.4 nm for both of the ALD materials. The roughness and

density values showed good nanolaminate structural quality with clear, consistent layers, and smooth interfaces. [35]

The TiO<sub>2</sub> layers are expected to be fully amorphous and this has been confirmed with ALD temperatures less than 210 °C together with single layer thicknesses less than 10 nm [35-37]. Aarik et al. reported that this is due to crystalline TiO<sub>2</sub> film growth starting with formation of amorphous transition layer, and deposition temperature of 350 °C was required to initiate anatase crystal structure formation for laminate thickness below 10 nm [36]. Moreover, Alasaarela et al. showed that with ALD Al<sub>2</sub>O<sub>3</sub> intermediate layer, the polycrystallinity related TiO<sub>2</sub> roughness can be decreased even at 350 °C TiO<sub>2</sub> deposition temperatures [38]. Indeed, no Raman peaks at 145 cm<sup>-1</sup> for anatase TiO<sub>2</sub> [39] were observed from any of the samples. Furthermore, the XRR measured level of density and surface roughness both support the presence of amorphous form of TiO<sub>2</sub> [40]. Al<sub>2</sub>O<sub>3</sub> is known to be amorphous below deposition temperature of 600 °C [41].

Fig. 1 shows EDS spectrum for the multilayer CrN/ALD nanolaminate samples (*default*) using 10.0 kV acceleration voltage. For samples without the ALD nanolaminate on top of CrN, the spectrum is otherwise identical, but there are no Ti-peaks.

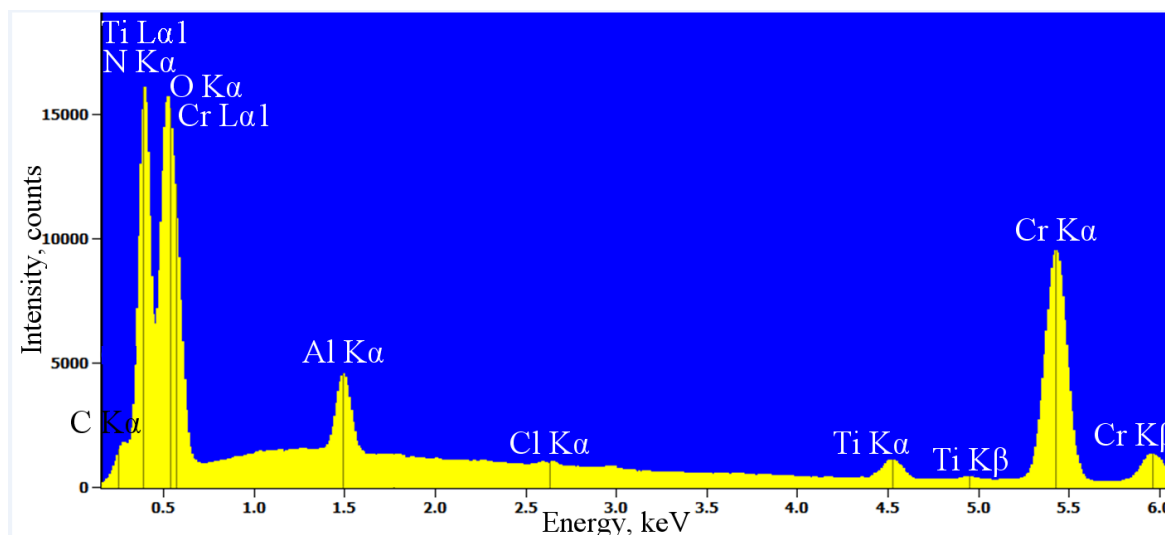


**Fig. 1:** EDS spectrum with 10.0 kV acceleration voltage for multilayer coating consisting of CrN and nanolaminate ALD of TiO<sub>2</sub> and Al<sub>2</sub>O<sub>3</sub> (*default*). Corresponding spectrum with CrN coating only is otherwise identical, except the Ti-peaks are not present.

### 3.2. Electrochemical properties

#### 3.2.1. Polarization curves

Fig. 2 presents the results of the electrochemical measurements. All the polarization curves shown are after 48 hours in the electrolyte and from the third potential sweep. Fig 2a shows polarization curves for three types of HSS samples: without coating, with the CrN coating and with a multilayer coating (*default*). In addition, polarization curves for the reference set of martensitic stainless steel and for the CrN coating itself (on glass substrate) are included in this Fig. 2. Passivation of the HSS – enabled by the high amount of alloying of W, Cr and Mo [42] (see Table 1) – is observed between -800 mV and -500 mV for non-coated samples. Passivation of the HSS is also observed for coated samples, though at less negative potentials. This passivation is observed already after 24 hours, but not with the first measurements after one hour. Passive film breakdown, observed as increase in current density, starts at approximately -400 mV for

the non-coated sample, and at about -200 mV for coated samples. With HSS/CrN/ALD nanolaminate samples, the corrosion current density starts to approach that of HSS/CrN after -200 mV. After -150 mV, the current density exceeds that of glass/CrN, showing there is at least some dissolution of the HSS. After -100 mV, the polarization curves of HSS/CrN and HSS/CrN/ALD nanolaminate are practically identical. It should be noted that this kind of increase in current density for HSS/CrN/ALD nanolaminate was already observed after 24 hours, but the protection by multilayer coating is still effective after 48 hours. This indicates that with sufficient overpotential there is some dissolution of steel through ALD coating at the bottom of pinholes, possibly through ALD coating defects, but the coating still mostly remains.

Tafel analysis shows that the corrosion current density is reduced by less than an order of magnitude with CrN coating, while multilayer coating results in almost two orders of magnitude decrease. From the corrosion potentials it can be observed that the ALD coating and the stainless steel are the noblest materials, while the HSS is the most active. The corrosion potential of HSS with a multilayer coating (*default*) is about the same as with the high-chromium martensitic stainless steel. For CrN coated steel disk, the corrosion potential has moved almost to that of the HSS (-920 mV), indicating the corrosion protection of CrN coating is almost completely lost. The corrosion potential of the multilayer coated steel disk is still noticeably higher than that of CrN coating on glass (-590 mV vs. -750 mV), showing that ALD coating is still intact and protecting at the top of CrN coating.

Fig. 2b shows the effect of plasma pre-treatment. Without plasma pre-treatment, the corrosion potential of the multilayer coated disk is close to that of CrN on glass (-720 mV vs -750 mV), indicating that ALD layer on CrN surface has no longer large coverage and CrN determines the corrosion potential. The improved corrosion

protection with plasma pre-treatment is probably due to cleaning of surface of impurities [25, 26], and possibly formation of thin, uniform oxide layer improving growth behavior [27]. Even without plasma pre-treatment, the corrosion current density is still noticeably lower than with only CrN coating (Fig. 2a), indicating that the ALD layer fills pinholes of the CrN layer. With plasma pre-treatment, the corrosion current density is still lower, though the difference is comparatively small. Identical results were obtained with the two different plasma pre-treatments.

Fig. 2c shows the effect of ALD layer thickness. With layer thickness of only 20 nm, the corrosion potential is lower – about the same as with CrN on glass. Although this difference is smaller than the standard deviation, increased exposed area without protection by ALD is confirmed by visual analysis after the LSV-measurements (chapter 3.2.2). The corrosion potentials of samples with 50 nm and 100 nm thick ALD nanolaminate are quite similar, indicating similar protection on CrN surface, but the current density with 100 nm thick ALD layer is less than half of that with 50 nm ALD nanolaminate – a much larger difference than obtained with the use of plasma pre-treatment. This indicates that while corrosion protection at CrN surface is about the same, the filling of CrN pinholes is drastically improved by this increase in ALD thickness. Improved corrosion protection by increased ALD layer thickness coincides with previous investigations [19,20].

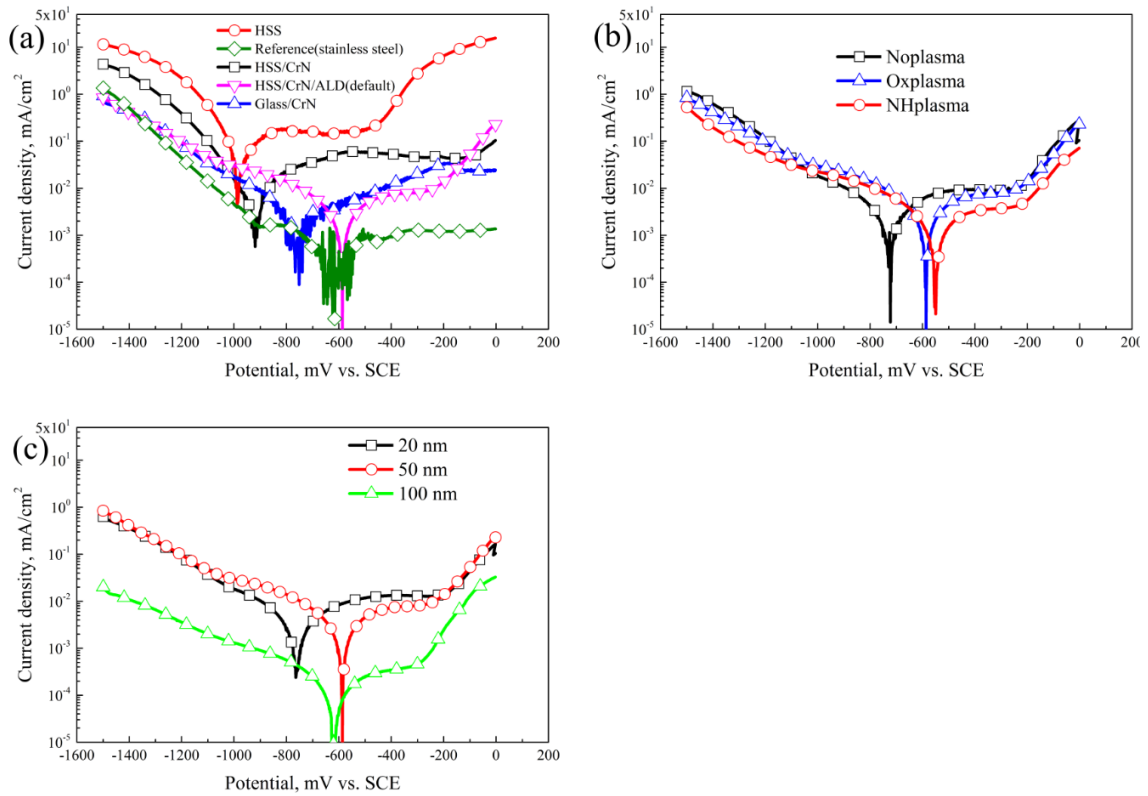


**Fig. 2:** Polarization results after 48 hours and three polarization sweeps a) Three types of HSS samples: without coating, with CrN coating and with multilayer coating. Polarization curves for reference martensitic stainless steel and for CrN coating itself (glass substrate) are also included b) multilayer coatings with different plasma pre-treatments c) multilayer coatings with different ALD-layer thicknesses.

For all the multilayer coated samples protective film breakdown – observed on the anodic side as increasing voltage after a flat area on the curve – occurs for all the multilayer samples at potential between -300 mV and -250 mV. This indicates that the overpotential is high enough to cause steel dissolution through the pinholes of the coating. This current increase was not seen on CrN on glass or stainless steel indicating that the effect is indeed the dissolution of the HSS substrate. This kind of breakdown was already observed for the second potential sweeps after 24 hours, but not with the first one.

Only results from last of the total three LSV measurements done for each sample type were presented in Fig. 2. Fig. 3, Fig. 4 and Fig. 5 show the results from all the

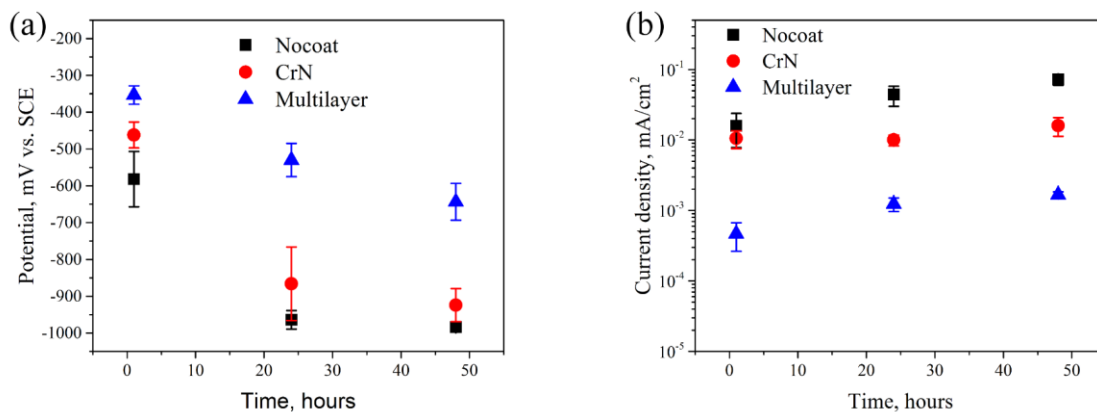
measurements for corrosion potential and corrosion current density by time. Each data point is averaged from three different LSV-measurements. Error bars are given as half of the difference between maximum and minimum values for corrosion potential, and as standard errors for corrosion current densities.

Fig. 3 compares the corrosion potential and corrosion current density increase by time with non-coated, CrN coated and CrN/ALD nanolaminate coated samples. With CrN coating only, the increase in corrosion potential is very minor between 24 and 48 hours, and the corrosion potential is close to that of non-coated steel. This indicates that the steel disks with only CrN coating are already mostly corroded after 24 hours.

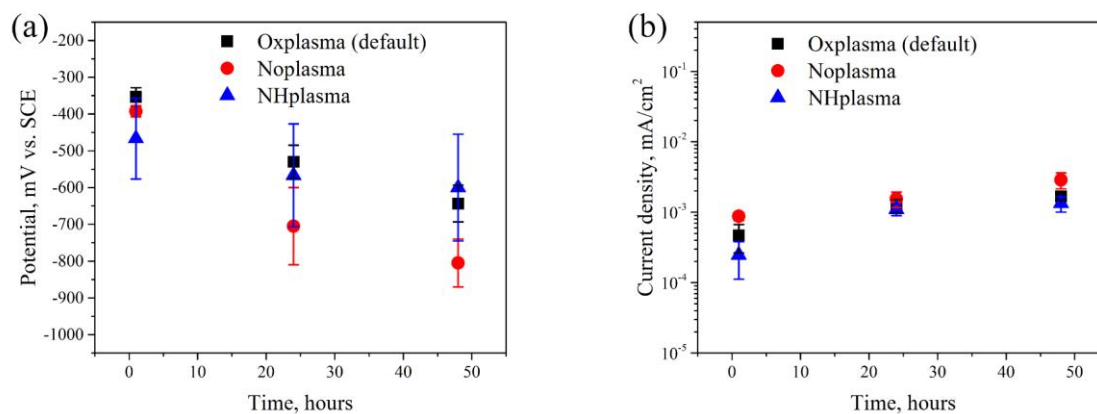
Fig. 4 shows the effect of plasma pre-treatment. On the first measurement after one hour, the corrosion potential is the same with or without plasma pre-treatment. After 24 and 48 hours, the corrosion potential without plasma pre-treatment is noticeably more negative, very close to that of with only CrN coating (see Fig. 3a). The corrosion current density is slightly larger without plasma pre-treatment. With the two different plasma pre-treatments, no differences can be distinguished.

Fig. 5 shows the effect of ALD layer thickness. The corrosion current density is inversely correlated to ALD layer thickness at all the measurement times. Corrosion potentials are identical within measurement variation for all the ALD layer thicknesses.

All the multilayer samples have between one and two orders of magnitude decrease in corrosion current densities compared to those with only CrN coating. The effect of increasing the ALD layer thickness resulting in reduced corrosion current density is most probably due to improved CrN pinhole filling. Corrosion potential becomes more negative and corrosion current density is increased by time for all the samples.



**Fig. 3:** a) Corrosion potential and b) corrosion current density by time for non-coated, CrN coated and CrN/ALD nanolaminate (*default*) coated steel disks. Each data point is averaged from three separate LSV-measurement.



**Fig. 4:** a) Corrosion potential and b) corrosion current density by time for steel disks without plasma pre-treatment, with oxygen plasma pre-treatment and with nitrogen/hydrogen plasma pre-treatment. Each data point is averaged from three separate LSV-measurement.

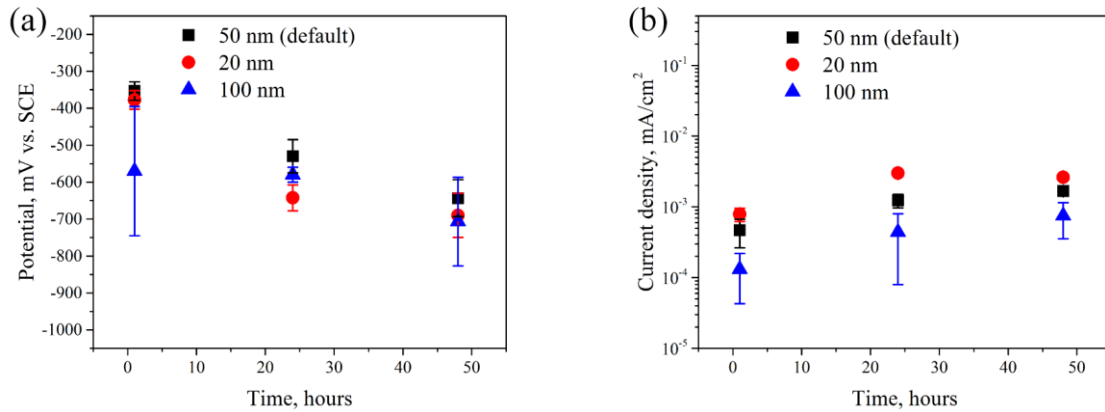


**Fig.5:** a) Corrosion potential and b) corrosion current density by time for CrN/ALD nanolaminate coated steel disks with different total ALD layer thicknesses. Each data point is averaged from three separate LSV-measurement.

Previous investigations have presented the polarization curves and decreases in current densities after only a short stabilization time and only with one potential sweep [11-17]. This corresponds to our measured values for the first potential sweep after one hour. In the first measurement, two order of magnitude decrease in current densities, compared to CrN coated samples, is obtained with plasma pre-treatment and 100 nm thick ALD layer, as seen from Fig. 5. In previous PVD/ALD on steel investigations, decreases by one order of magnitude with single ALD layer have been reported [15,17]. Härkönen et al. reported over two orders of magnitude decrease in corrosion current density with Al<sub>2</sub>O<sub>3</sub>/Ta<sub>2</sub>O<sub>5</sub> nanolaminate coatings on PVD CrN coatings [12]. Comparing the current investigations to those presented by other authors, it should be noted that conducting multiple LSV-sweeps increases the corrosion current densities and amount of rust in sample surfaces.

### 3.2.2. Corrosion resistance

Fig. 6 shows the results for visual estimation of different samples after 48 hours in electrolyte and three potential sweeps. Samples without any coating or only CrN coating are corroded on the whole contact area to the electrolyte. Of the different multilayer samples, those without plasma pre-treatment and those with only 20 nm thick ALD layer also have a large amount of corrosion. The best protection is obtained by using plasma pre-treatment and 100 nm ALD coating: in this case corrosion is only observable at the middle pit of the disk.

The ALD coatings did not change color after 48 in salt solution. This shows there is no significant dissolution of the coating at the top of the CrN surface, as the reduced thickness would show as a change in color. Diaz et al. reported very high 7 nm/ h dissolution rate for of  $\text{Al}_2\text{O}_3$  on steel and proposed that this was due cathodic reduction of dissolved oxygen at steel interface in ALD defects, greatly increasing pH, and thus causing heavy  $\text{Al}_2\text{O}_3$  dissolution [24]. Considering the case of  $\text{Al}_2\text{O}_3/\text{TiO}_2$  nanolaminate at bottom of high aspect ratio pinholes, dissolution products could be expected to result in drastic increases in local pH. Though basic conditions could cause high dissolution rates for  $\text{Al}_2\text{O}_3$ , the  $\text{TiO}_2$  layer on top is expected to remain unaffected even in very basic environments [43].

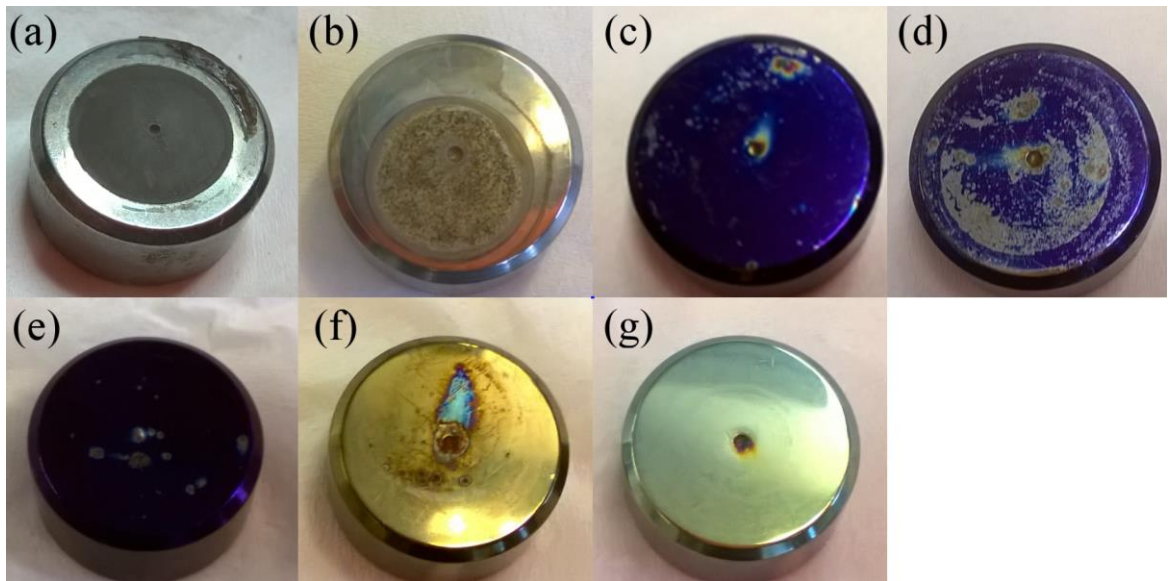


**Fig. 6:** Photographs of samples after 48 hours in electrolyte and three potential sweeps for a) non-coated b) CrN coated c) *default* d) Noplasma e) NHplasma f) t20nm g) t100nm samples.

Fig. 7 shows middle of the pit before corrosion procedure – a noticeably large amount of cracks is observed in the CrN coating. These cracks lead into more aggressive corrosion at the pit: Panjan et al. have previously reported that surface irregularities can lead into increased defect density for PVD coatings [44]. We observed that the rust originating from the pit was generally into direction of gravity in the electrochemical cell setup. This effect can be explained by higher density of the concentrated metal-containing solution inside the pit [45]. The effect was most clearly observed with 20 nm ALD coating thickness (Fig. 6f).

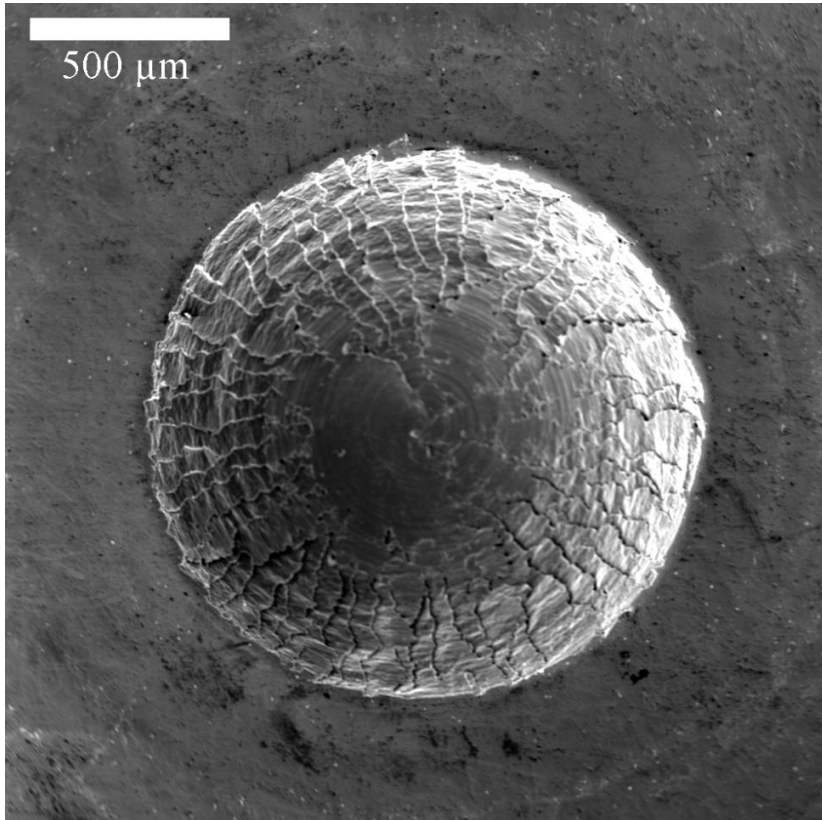


**Fig. 7:** SEM image of the middle pit of CrN coated steel disk: large amount of cracks in CrN coating cause the pit to be prone to corrosion.

The results of the LSV-investigations with the middle pit covered by protective lacquer are shown in Fig. 8. Here the averaged results of our main LSV measurements (see Fig. 3) are compared to samples with the middle pit covered by lacquer. Without lacquering, corrosion potential becomes more negative and corrosion current density increases by time for all the samples during 48 h test period. With lacquering, both the corrosion current density and corrosion potential remain approximately constant with the lacquered CrN/ALD nanolaminate samples. The differences between lacquered and non-lacquered multilayer samples are very small and the performance of non-lacquered CrN/ALD nanolaminate is superior to lacquered CrN. Compared to multilayer samples, the differences between lacquered and non-lacquered CrN coated samples are much more significant. Without lacquering, the corrosion potential of CrN coated steel disks

is close to that of uncoated after 24 hours (-900 mV vs. -950 mV). With lacquering, the corrosion potential has not stabilized after 48 hours, unlike in the case of without lacquering. After the LSV-measurements, visual estimation also shows that the steel disks surface is not completely rusted like in the case of without lacquering. We conclude that the cracks at the CrN layer at middle pit significantly reduce the corrosion protection of this PVD coating, but the bottom of these cracks is protected by the ALD coating.

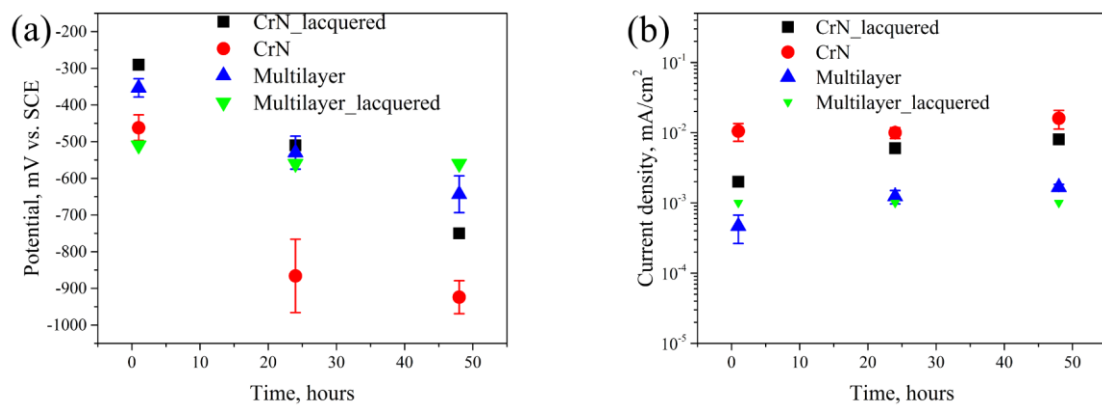


**Fig. 8:** a) Corrosion potentials by time b) corrosion current densities by time for CrN and CrN/ALD nanolaminate (*default*) coated steel disks with and without lacquering of the middle pit.

Results for NSS tests after 48 hours for three different dental curettes are shown in Fig. 9. The curettes without coating are completely rusted. For the coated curettes, some rust spots are observed at the shank and a noticeably large amount of rust is observed at the lateral surface of the cutting edge, denoted by arrow in the image. The larger amount of rust is most probably due to higher surface roughness at the lateral surface. The higher surface roughness has been shown to detrimentally affect both the protection of PVD [10] and ALD [18] coatings. The amount of rust is larger on curettes with only CrN coating, but the difference is much smaller than with the steel disks visually evaluated after LSV-measurements (Fig. 6).

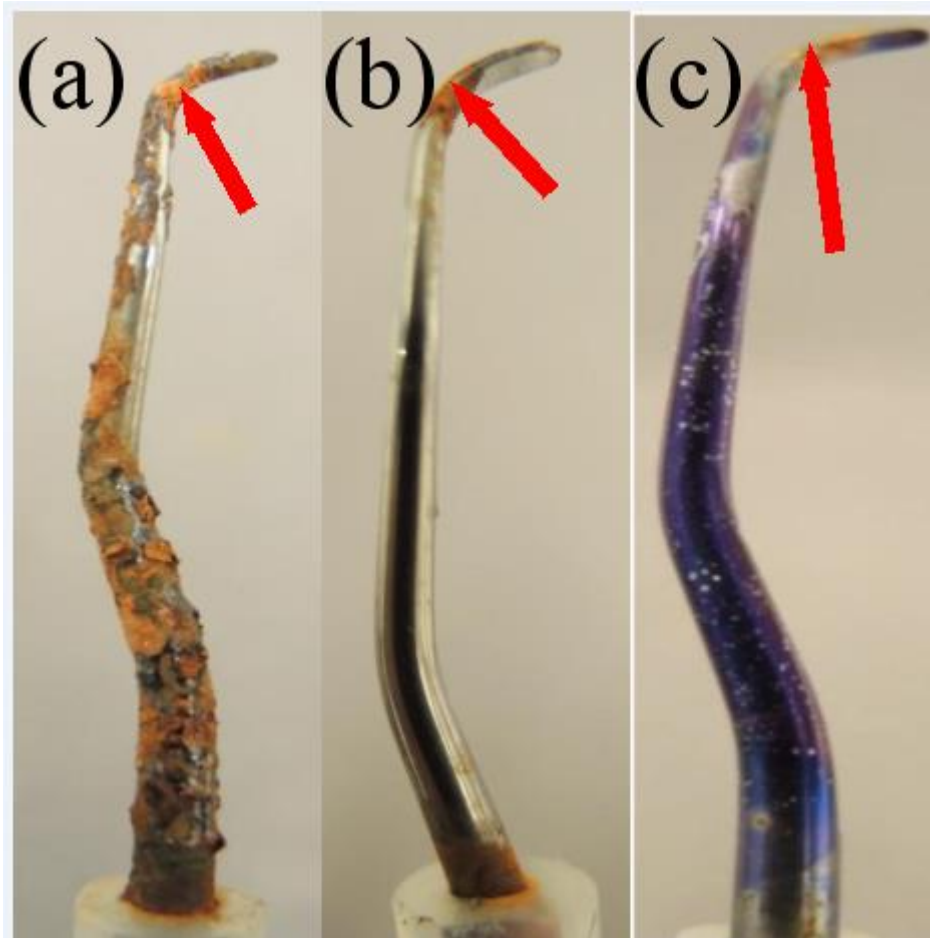


**Fig. 9:** HSS dental curettes after 48 hours in NSS testing: a) non-coated b) CrN coated c) CrN/ALD nanolaminate (*default*). Arrow denotes lateral surface of the curette, where the surface roughness of the tool is higher.

Several of the previous investigations on corrosion protection of steel by multilayer or ALD coatings have not evaluated corrosion resistance after an extended period of time, though Härkönen et al. [12] used ISO 9227 standard neutral salt spray (NSS) tests for evaluation of corrosion durability of their CrN/ALD nanolaminate coatings. With the harsher test conditions used (50 g/l compared to our 10 g/l), they observed their CrN coated AISI 52100 steel heavily corroded already after two hours, while some of the CrN/ALD nanolaminate samples remained corrosion free even after 168 hours. The difference between CrN coating only and CrN/ALD nanolaminate was thus much more drastic than in our investigations. It is difficult to directly compare these results to ours

due to differences in test conditions and samples – the effect of 3D-shape and surface roughness require future investigations, as the research has thus far focused mostly on planar substrates.

### **3.3. Sealing properties**

The estimated porosities of the coatings are presented in Table 3. The current densities are calculated using equation (1) and results from electrochemical measurements (chapter 3.2.1), using corrosion current density values at the corrosion potential after one hour. For multilayer CrN/ALD nanolaminates, the value for  $i_{coating}$  is approximated to be zero. Using microscope analysis of the defect area and using the current density calculation give greatly differing results. Considering the large deviation in optical microscope analysis, we can only conclude that the area classified as defects at sample surface is about 5 %, both with and without the ALD coating. This is similar to that of reported previously for PVD CrN coating with this analysis method [30]. This method evaluates the porosity only based on top view of the sample, and does not take into account high localized corrosion of less noble substrate [10].

Using the current density calculation (equation 1) gives porosity of one order of magnitude higher for the CrN coating. Values this high have been reported previously for magnetron sputtered Ti coatings [31], TiN coating deposited by cathodic arc evaporation (CAE) [46] and TaO coating deposited by filtered CAE [21]. For CAE-deposited CrN coating, Creus et al. reported 9 % porosity [46]. Tato et al. suggest that dissolution and undercutting at the bottom of the pores can lead into larger values by this method [31]. Based on undercutting observed in FIB cross-sections of corroded CrN coated steel disk (see Fig 10) this seems a very plausible explanation for the extremely large value for the CrN coated samples in our tests. For multilayer PVD coatings, values of 1 % or smaller have been reported [21,31,44], and porosities as low

as 0.04 % have been reported with PVD nanolaminate/ALD nanolaminate coatings [21]. Our results show that increasing the thickness of the ALD coating reduces the porosity of the CrN-coating, with porosities below 1% obtained with 100 nm thick ALD nanolaminates.

**Table 3:** Coating porosities estimated by two different methods: topview optical microscope analysis and corrosion current density calculation.

Coating	Porosity (%) by optical microscope	Porosity (%) by current density
CrN	$4.8 \pm 2.0$	$57 \pm 19$
t20nm		$5.0 \pm 1.0$
<i>default</i> (50 nm)		$3.0 \pm 1.3$
t100nm	$5.8 \pm 1.4$	$0.8 \pm 0$

Fig. 10 shows a cross-sectional image taken from a pinhole. The carbides of the HSS are quite easily observable. The CrN coating is present at the bottom of the pinhole, though its thickness is only about 1  $\mu\text{m}$ . Fig. 11 shows a closer magnification of the CrN/ALD nanolaminate stack at the bottom of the pinhole. PVD CrN coating has been reported to grow in form of columns consisting of different grains, with voids or amorphous areas between the columns [30]. A possible intercolumnar void is seen at the bottom CrN layer in Fig. 11. This kind of open porosity can act as localized anode where corrosion starts [10].

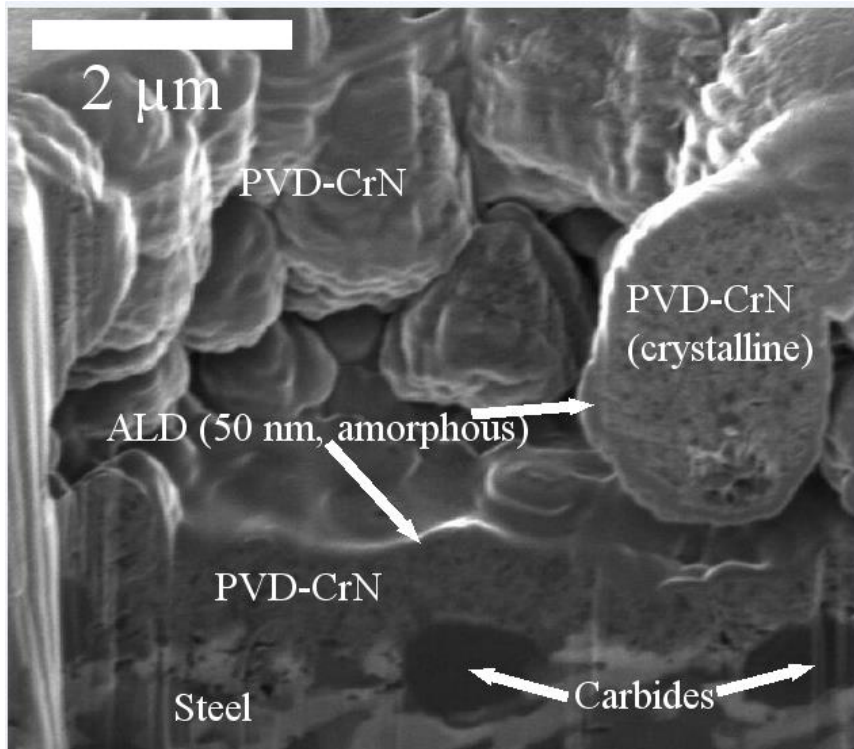


**Fig. 10:** Cross-sectional image taken from CrN pinhole, from the multilayer PVD/ALD nanolaminate sample (*default*).

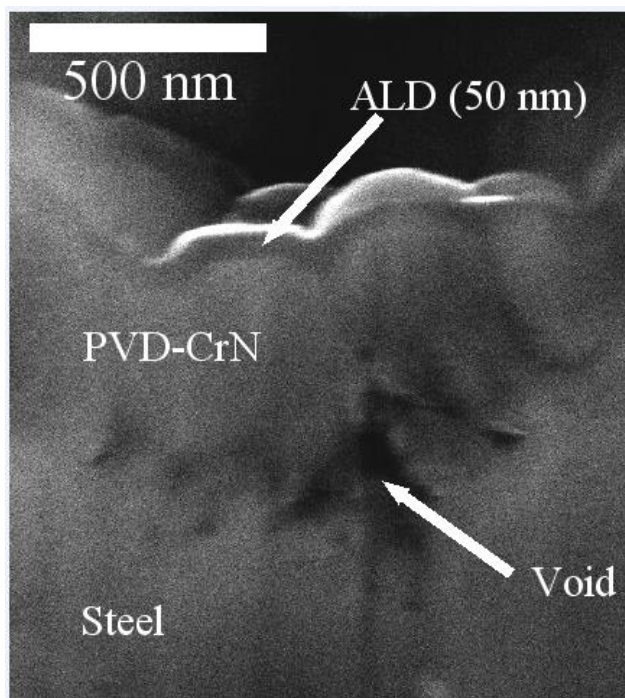


**Fig. 11:** Cross-sectional image taken from CrN pinhole, from the multilayer PVD/ALD nanolaminate sample (*default*), with higher magnification.

FIB cross-sections were also made of two samples after 24 hours in the electrolyte and two LSV-sweeps. Fig. 12 and Fig. 13 show top view (before taking cross-section) and cross-sectional images for samples with only a CrN coating and with a CrN/ALD nanolaminate ( $t_{100\text{nm}}$ ) coating, respectively. For the sample with only CrN coating, the corrosion has progressed preferentially to one specific direction from the pinhole. Some amount of corrosion is observed for the CrN/ALD nanolaminate below the coating, but the pinhole itself appears sealed. The width of the pinhole is slightly more than double of ALD-layer thickness (240 nm vs. 200 nm), and it is plausible that although the ALD coating was not sufficiently thick to completely seal the pinhole, the corrosion products have sealed the pinhole.

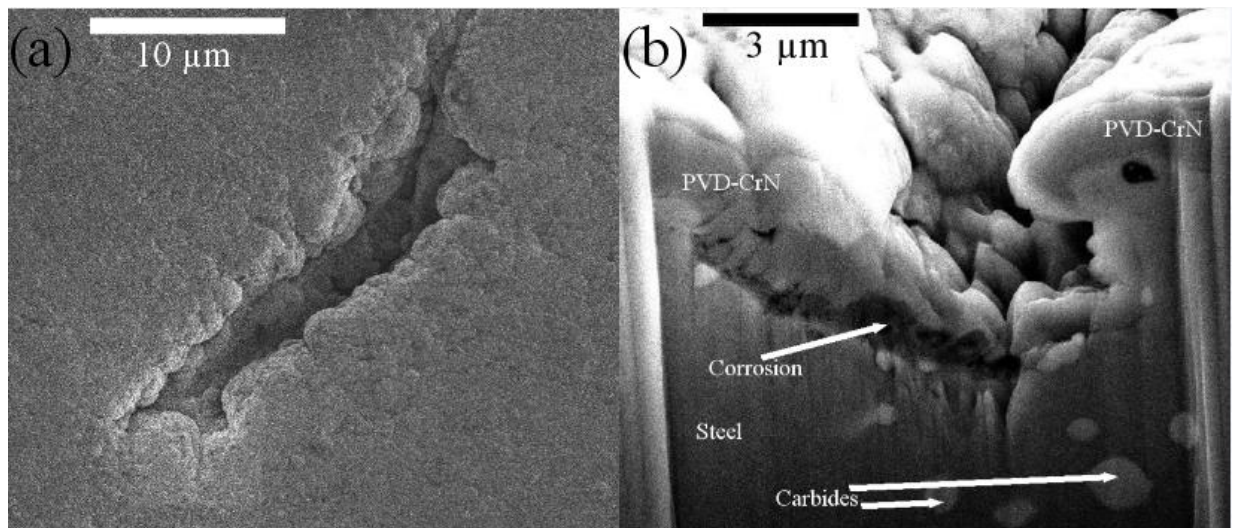


**Fig. 12:** Micrographs of CrN coated steel disk after 24 hours in the electrolyte and two potential sweeps a) top view of a pinhole before cross-sectioning b) cross-section of the pinhole.

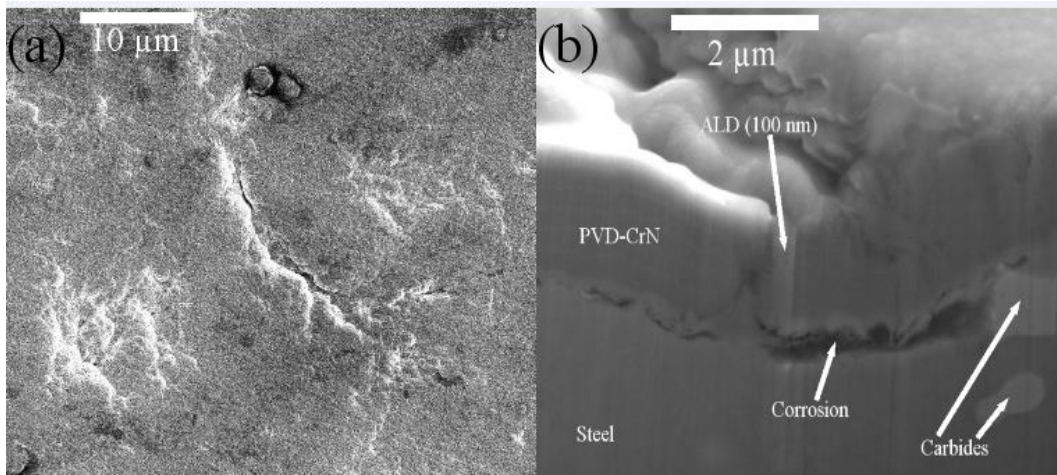


**Fig. 13:** Micrographs of CrN/ALD nanolaminate (t100nm) coated steel disk after 24 hours in the electrolyte and two potential sweeps a) top view of a pinhole before cross-sectioning b) cross-section of the pinhole.

### 3.4. Adhesion of CrN and ALD coatings

Adhesion of CrN coating was found to conform with adherence class HF1, with very few or zero cracks near the indentation. The good adherence quality is as expected from a commercial PVD coating.

Not using plasma pre-treatment results in poor adhesion of ALD-layers as seen in Fig. 14a : the ALD-layer has been removed from the vicinity (~ 0.2 mm) of the Rockwell indentation. In contrast, for all the samples with plasma pre-treatment, the ALD-layer remains at the vicinity of the indentation, as shown in Fig. 14b. For samples without plasma pre-treatment, there was no signal observed for titanium (see Fig. 1), confirming that the ALD nanolaminate is removed from the vicinity of the indentation. With plasma pre-treatment, the measured spectrum was the same at the vicinity of indentation as it was at the rest of the disk area.

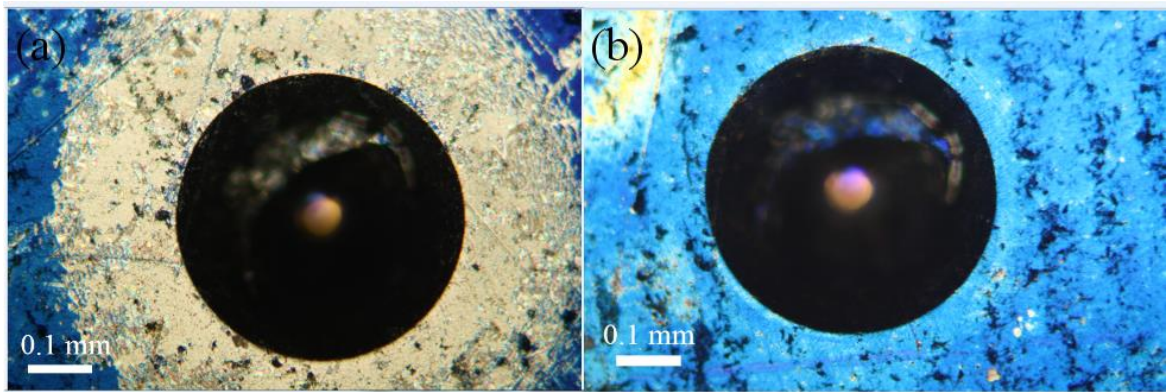


**Fig. 14:** Optical microscope image of Rockwell indents for evaluation of ALD coating adhesion a) without plasma pre-treatment b) with plasma pre-treatment (*default*). All the samples with plasma pre-treatment showed similar results.

#### **4. Conclusions**

Multilayer CrN/ALD nanolaminate coatings were applied to high speed steel for improved corrosion protection. Pinholes in hard CrN coating on HSS were sealed with ALD Al<sub>2</sub>O<sub>3</sub>/TiO<sub>2</sub> nanolaminate. This decreased corrosion current density by approximately two orders of magnitude. Increasing the thickness of the ALD layer from 50 nm to 100 nm improved pinhole sealing and corrosion protection. Plasma pre-treatment prior to ALD deposition was shown to improve corrosion protection and especially adhesion of ALD layer. Conformal sealing by ALD layers at the bottom of the pinholes was confirmed by FIB/SEM-technique. Use of multilayer coatings for corrosion protection can allow harder base steel material be chosen for high-value applications, where both excellent mechanical properties and corrosion resistance are required.

#### **Acknowledgements**

The work has been done within the FIMECC HYBRIDS (Hybrid Materials) programme as part of the FIMECC Breakthrough Materials Doctoral School. We

gratefully acknowledge the financial support from the Finnish Funding Agency for Innovation (Tekes) and the participating companies. The ALD depositions and the nanolaminate-on-silicon characterizations were carried out in the Micronova cleanroom facility of Aalto University. The NSS tests were conducted at Tampere University of Technology by Merja Ritola in conjunction with a larger NSS test set. Raman spectroscopy analysis for crystallinity of nanolaminates was conducted by Ajai Iyer. Authors would like to thank Sakari Sintonen for the help with the XRR analysis, and Toni Luoto for information and advice provided regarding the dental cures.

## References

- [1] J. Leppaniemi, J. Lyytinen, O. Elomaa, K. Suomalainen, J. Koskinen, The influence of PVD coatings on the wear performance of steel dental cures, *Key Eng. Mater.* 674 (2016) 289-295.
- [2] P.J. Kelly, R.D. Arnell, Magnetron sputtering: a review of recent developments and applications, *Vac.* 56.3 (2000) 159-172.
- [3] K. Holmberg, A. Matthews, *Coatings Tribology: Properties, Mechanisms, Techniques and Applications in Surface Engineering*, second ed., Elsevier, Amsterdam, 2009
- [4] T. Hurkmans, D.B. Lewis, J.S. Brooks, W.-D. Münz, Chromium nitride coatings grown by unbalanced magnetron (UBM) and combined arc/unbalanced magnetron (ABS™) deposition techniques, *Surf. & Coat. Technol.* 86 (1996) 192-199.
- [5] C. Mendibide, P. Steyer, J.-P. Millet, Formation of a semiconductive surface film on nanomultilayered TiN/CrN coatings and its correlation with corrosion protection of steel, *Surf. & Coat. Technol.* 200.1 (2005) 109-112.

- [6] B. Navinšek, P. Panjan, I. Milošev, Industrial applications of CrN (PVD) coatings, deposited at high and low temperatures, *Surf. & Coat. Technol.* 97.1 (1997) 182-191.
- [7] C. Liu, Q. Bi, A. Matthews, EIS comparison on corrosion performance of PVD TiN and CrN coated mild steel in 0.5 N NaCl aqueous solution, *Corros. Sci.* 43.10 (2001) 1953-1961.
- [8] P. Panjan, D.K. Merl, F. Zupanič, M. Čekada, M. Panjan, SEM study of defects in PVD hard coatings using focused ion beam milling, *Surf. & Coat. Technol.* 202.11 (2008) 2302-2305.
- [9] H.A. Jehn, Improvement of the corrosion resistance of PVD hard coating–substrate systems, *Surf. & Coat. Technol.* 125.1 (2000) 212-217.
- [10] M. Fenker, M. Balzer, H. Kappl, Corrosion protection with hard coatings on steel: Past approaches and current research efforts, *Surf. & Coat. Technol.* 257 (2014) 182-205
- [11] E. Marin, L. Guzman, A. Lanzutti, L. Fedrizzi, M. Saikkonen, Chemical and electrochemical characterization of hybrid PVD+ALD hard coatings on tool steel, *Electrochem. Commun.* 11.10 (2009) 2060-2063.
- [12] E. Härkönen, I. Kolev, B. Díaz, J. Światowska, V. Maurice, A. Seyeux, P. Marcus, M. Fenker, L. Toth, G. Radnoczi, M. Vehkamäki, M. Ritala, Sealing of hard CrN and DLC coatings with atomic layer deposition, *ACS Appl. Mater. Interfaces* 6.3 (2014) 1893-1901.
- [13] E. Marin, L. Guzman, A. Lanzutti, W. Ensinger, L. Fedrizzi, Multilayer Al<sub>2</sub>O<sub>3</sub>/TiO<sub>2</sub> atomic layer deposition coatings for the corrosion protection of stainless steel, *Thin Solid Films* 522 (2012) 283-288.

- [14] E. Härkönen, B. Díaz, J. Światowska, V. Maurice, A. Seyeux, M. Vehkamäki, T. Sajavaara, M. Fenker, P. Marcus, M. Ritala, Corrosion protection of steel with oxide nanolaminates grown by atomic layer deposition, *J. Electrochem. Soc.* 158.11 (2011) C369-C378.
- [15] E. Marin, A. Lanzutti, L. Guzman, L. Fedrizzi, Corrosion protection of AISI 316 stainless steel by ALD alumina/titania nanometric coatings, *J. Coat. Technol. & Res.* 8.5 (2011) 655-659.
- [16] E. Härkönen, S. E. Potts, W.M.M. Kessels, B. Díaz, A. Seyeux, J. Światowska, V. Maurice, P. Marcus, G. Radnoczi, L. Toth, M. Kariniemi, J. Niinistö, M. Ritala, Hydrogen–argon plasma pre-treatment for improving the anti-corrosion properties of thin Al<sub>2</sub>O<sub>3</sub> films deposited using atomic layer deposition on steel, *Thin Solid Films* 534 (2013) 384-393.
- [17] C.X. Shan, X. Hou, K.-L. Choy, P. Choquet, Improvement in corrosion resistance of CrN coated stainless steel by conformal TiO<sub>2</sub> deposition, *Surf. & Coat. Technol.* 202.10 (2008) 2147-2151.
- [18] B. Díaz, E. Härkönen, J. Światowska, A. Seyeux, V. Maurice, M. Ritala, P. Marcus, Corrosion properties of steel protected by nanometre-thick oxide coatings, *Corros. Sci.* 82 (2014) 208-217.
- [19] S. E. Potts, L. Schmalz, M. Fenker, B. Díaz, J. Światowska, V. Maurice, A. Seyeux, P. Marcus, G. Radnoczi, L. Toth, W.M.M. Kessels, Ultra-thin aluminium oxide films deposited by plasma-enhanced atomic layer deposition for corrosion protection, *J. Electrochem. Soc.* 158.5 (2011) C132-C138.
- [20] B. Díaz, E. Härkönen, J. Światowska, V. Maurice, A. Seyeux, P. Marcus, M. Ritala, Low-temperature atomic layer deposition of Al<sub>2</sub>O<sub>3</sub> thin coatings for

- corrosion protection of steel: surface and electrochemical analysis, *Corros. Sci.* 53.6 (2011) 2168-2175.
- [21] E. Härkönen, S. Tervakangas, J. Kolehmainen, B. Diaz, J. Światowska, V. Maurice, A. Seyeux, P. Marcus, M. Fenker, L. Toth, G. Radnoczi, M. Ritala, Interface control of atomic layer deposited oxide coatings by filtered cathodic arc deposited sublayers for improved corrosion protection, *Mater. Chem. & Phys.* 147.3 (2014) 895-907.
- [22] S.M. George, Atomic layer deposition: an overview, *Chem. Rev.* 110.1 (2009): 111-131.
- [23] M. Ritala, M. Leskelä, J.-P. Dekker, C. Mutsaers, P.J. Soininen, J. Skarp, Perfectly conformal TiN and Al<sub>2</sub>O<sub>3</sub> films deposited by atomic layer deposition, *Chem. Vap. Depos.* 5.1 (1999) 7-9.
- [24] B. Díaz, E. Härkönen, V. Maurice, J. Światowska, A. Seyeux, M. Ritala, P. Marcus, Failure mechanism of thin Al<sub>2</sub>O<sub>3</sub> coatings grown by atomic layer deposition for corrosion protection of carbon steel, *Electrochimica Acta* 56.26 (2011) 9609-9618.
- [25] H. Steffen, J. Schwarz, H. Kersten, J.F. Behnke, C. Eggs, Process control of RF plasma assisted surface cleaning, *Thin Solid Films* 283.1 (1996) 158-164.
- [26] P. Krüger, R. Knes, J. Friedrich, Surface cleaning by plasma-enhanced desorption of contaminants (PEDC), *Surf. & Coat. Technol.* 112.1 (1999) 240-244.
- [27] J. Yang, S. Kim, W. Choi, S.H. Park, Y. Jung, M.H. Cho, H. Kim, Improved growth behavior of atomic-layer-deposited high-k dielectrics on multilayer MoS<sub>2</sub> by oxygen plasma pretreatment, *ACS Appl. Mater. Interfaces* 5.11 (2013) 4739-4744.

- [28] J. Tiilikainen, J.M. Tilli, V. Bosund, N. Mattila, T. Hakkarainen, V.M. Airaksinen, H. Lipsanen, Nonlinear fitness–space–structure adaptation and principal component analysis in genetic algorithms: an application to x-ray reflectivity analysis, *J. Phys. D: Appl. Phys.* 40.1 (2006) 215.
- [29] ASTM G. 59–97, Standard Test Method for Conducting Potentiodynamic Polarization Resistance Measurements, Am. Soc. Test. & Mater., 1997.
- [30] L. Cunha, M. Andritschky, K. Pischow, Z. Wang, Microstructure of CrN coatings produced by PVD techniques, *Thin Solid Films* 355 (1999) 465-471.
- [31] W. Tato, D. Landolt, Electrochemical determination of the porosity of single and duplex PVD coatings of titanium and titanium nitride on brass, *J. Electrochem. Soc.* 145.12 (1998) 4173-4181.
- [32] C.A. Volkert, A.M. Minor, Focused ion beam microscopy and micromachining, *MRS bulletin* 32.05 (2007) 389-399.
- [33] W. Heinke, A. Leyland, A. Matthews, G. Berg, C. Friedrich, E. Broszeit, Evaluation of PVD nitride coatings, using impact, scratch and Rockwell-C adhesion tests, *Thin Solid Films* 270.1 (1995) 431-438.
- [34] S. Zaitso, S. Motokoshi, T. Jitsuno, M. Nakatsuka, T. Yamanaka, Large-Area Optical Coatings with Uniform Thickness Grown by Surface Chemical Reactions for High-Power Laser Applications, *J. Appl. Phys.* 41 (2002) 160-165.
- [35] S. Sintonen, S. Ali, O.M.E. Ylivaara, R.L. Puurunen, H. Lipsanen, XRR characterization of ALD  $\text{Al}_2\text{O}_3/\text{TiO}_2$  nanolaminates with ultra-thin bilayers, *J. Vac. Sci. Technol. A* 32 (2014) 01A111.
- [36] J. Aarik, A. Aidla, T. Uustare, V. Sammelselg, Morphology and Structure of  $\text{TiO}_2$  Thin Films Grown by Atomic Layer Deposition, *J. Cryst. Growth* 148 (1995) 268-275.

- [37] V. Fedorenko, I. Iatsunskyi, M. Pavlenko, M. Jancelewicz, E. Coy, R. Viter, Structural and optical properties of TiO<sub>2</sub>-Al<sub>2</sub>O<sub>3</sub> nanolaminates produced by atomic layer deposition, SPIE Security+ Defence, Intern. Soc. Opt. and Photonics (2015) 96490X-96490X-6.
- [38] T. Alasaarela, J. Saastamoinen, A. Hiltunen, A. Säynätjoki, A. Tervonen, P. Stenberg, M. Kuittinen, S. Honkanen, Atomic layer deposited titanium dioxide and its application in resonant waveguide grating, Appl. Opt. 49 (2010) 4321-4325.
- [39] I. Iatsunskyi, M. Jancelewicz, G. Nowaczyk, M. Kempniński, B. Peplińska, M. Jarek, K. Załęski, S. Jurga, V. Smyntyna, Atomic layer deposition TiO<sub>2</sub> coated porous silicon surface: Structural characterization and morphological features, Thin Solid Films 589 (2015) 303-308.
- [40] J. Aarik, A. Aidla, H. Mändar, V. Sammelseg, Anomalous effect of temperature on atomic layer deposition of titanium dioxide, J. Crys. Growth 220.4 (2000) 531-537.
- [41] V. Miikkulainen, M. Leskelä, M. Ritala, R.L. Puurunen, Crystallinity of inorganic films grown by atomic layer deposition: Overview and general trends, J. Appl. Phys. 113.2 (2013) 021301.
- [42] V.A. Alves, C.M.A. Brett, Influence of alloying on the passive behaviour of steels in bicarbonate medium, Corros. Sci. 44.9 (2002) 1949-1965.
- [43] G.C. Correa, B. Bao, N.C. Strandwitz, Chemical Stability of Titania and Alumina Thin Films Formed by Atomic Layer Deposition, ACS Appl. Mater. Interfaces 7.27 (2015) 14816-14821.
- [44] P. Panjan, M. Čekada, M. Panjan, D. Kek-Merl, Growth defects in PVD hard coatings, Vac. 84.1 (2009) 209-214

- [45] A. Hassel, J. Schultze, Passivity of Metals, Alloys, and Semiconductors, in: A.J. Bard, M. Stratmann, G.S. Frankel, Encyclopedia of Electrochemistry, Corrosion and Oxide Films, Vol. 4, Wiley-VCh, 2003, p.220.
- [46] J. Creus, H. Mazille, H. Idrissi, Porosity evaluation of protective coatings onto steel, through electrochemical techniques, Surf. & Coat. Technol. 130.2 (2000) 224-232.